Supplementary Information

S1 Study site and sampling

All sites were located in shallow littoral areas with a total water depth of approximately 1 – 2 m. Water samples were collected at 0.5 – 1 m depth. Dissolved CH_4 concentrations, sediment-water CH_4 fluxes, potential CH_4 production and carbon stable isotopes were determined during the four seasonal campaigns. Sediment organic carbon was determined in spring, summer, and autumn. Sampling details for each site are provided in Table S1.

S2 Correction and calibration of stable carbon isotope measurements

For the correction and calibration of the CO_2 measurements, we injected variable volumes of a standard gas of $\delta^{13}C\text{-}CO_2$ (-8.6 ± 0.3 ‰, AirLiquide GmbH, Germany) into the SSIM to be diluted to ratios between 40 ppm and 400 ppm CO_2 (Fig. S1a). The measured $\delta^{13}C\text{-}CO_2$ were used to create a calibration curve similar to Uhlig and Loose (2017). Briefly, the best fit of a linear regression of the logarithm of methane mixing ratio ln (p (CO_2)) was used as empirical correction for the sample measurements (Fig. S1b). Based on the results, all measurements with a partial pressure p($^{12+13}CO_2$) below 400 ppm were corrected as follows:

$$\delta^{13}CO_2 corrected = \delta^{13}CO_2 measured - \Delta\,\delta^{13}CO_2 \qquad \text{(S1)}$$

and

$$\Delta\,\delta^{13}CO_2 = m_{fit} \times \ln(p(^{12+13}CO_2)) + a_{fit} \qquad \text{(S2)}$$

with $\Delta\delta^{13}C\text{-}CO_2$ being the isotope ratio residuals, m_{fit} the slope of logarithmic empirical fit, and a_{fit} the y-intercept of logarithmic empirical fit.

We estimated the apparent fractionation factor (α_{app}) for the gas samples retrieved from water and sediment samples following Conrad et al. (2009). The apparent fractionation factor is defined using Eq. (S3) as

$$\propto app = (\delta^{13}C - CO_2 + 10^3)/\,(\delta^{13}C - CH_4 + 10^3) \qquad \text{(S3)}$$

where $\delta^{13}C\text{-}CH_4$ and $\delta^{13}C\text{-}CO_2$ were measured with the CRDS as described above.

Supplementary tables

Table S1. Sampling dates, coordinates, basin assignments, and water and sediment temperatures at each site. Tw and Ts denote water and sediment temperature, respectively.

Site	Lake	UTM E [m]	UTM N [m]	Spring date	Spring Tw [°C]	Spring Ts [°C]	Summer date	Summer Tw [°C]	Summer Ts [°C]	Autumn date	Autumn Tw [°C]	Autumn Ts [°C]	Winter date	Winter Tw [°C]	Winter Ts [°C]
OBG	ULC	514303	5282946	08.04.2024	13	10	30.07.2024	23	23	31.10.2024	13	12	17.12.2024	8	7
SIP	ULC	507776	5293267	14.05.2024	15	16	30.07.2024	23	23	31.10.2024	13	12	17.12.2024	8	7
MUN	ULC	517848	5275825	12.04.2024	8	10	31.07.2024	24	23	05.11.2024	12	9	18.12.2024	7	7
LBM	ULC	530024	5279166	12.04.2024	10	10	31.07.2024	22	23	05.11.2024	12	12	16.12.2024	7	7
G1	LLC	503883	5283484	25.05.2024	18	16	09.08.2024	25	25	22.10.2024	15	15	12.12.2024	6	6
G2	LLC	506665	5283643	25.05.2024	19	18	09.08.2024	26	26	22.10.2024	14	15	12.12.2024	6	6
G3	LLC	500200	5286419	25.05.2024	16	17	09.08.2024	24	24	22.10.2024	14	14	12.12.2024	6	6

Table S2. Apparent carbon isotope fractionation factors (α_{app}) in water across sampling sites and seasons.

Site	Spring	Summer	Autumn	Winter
OBG	1.066 ± 0.002	1.071 ± 0.004	1.054 ± 0.004	1.031 ± 0.006
SIP	1.077 ± 0.008	1.071 ± 0.010	1.056 ± 0.009	1.037 ± 0.007
MUN	1.063 ± 0.008	1.063 ± 0.004	1.055 ± 0.005	1.036 ± 0.004
LBM	1.073 ± 0.009	1.075 ± 0.003	1.051 ± 0.004	1.034 ± 0.009
G1	1.078 ± 0.004	1.085 ± 0.008	1.044 ± 0.007	1.033 ± 0.006
G2	1.074 ± 0.004	1.071 ± 0.012	1.055 ± 0.004	1.025 ± 0.003
G3	1.073 ± 0.002	1.063 ± 0.010	1.044 ± 0.005	1.033 ± 0.007

Table S3. Apparent carbon isotope fractionation factors (α_{app}) in sediment across sampling sites and seasons.

Site	Spring	Summer	Autumn	Winter
OBG	1.075 ± 0.007	1.057 ± 0.002	1.050 ± 0.005	1.046 ± 0.003
SIP	1.067 ± 0.006	1.052 ± 0.005	1.049 ± 0.002	1.052 ± 0.002
MUN	1.063 ± 0.005	1.049 ± 0.001	1.052 ± 0.004	1.048 ± 0.003
LBM	1.063 ± 0.004	1.049 ± 0.002	1.049 ± 0.004	1.034 ± 0.003
G1	1.059 ± 0.003	1.048 ± 0.003	1.052 ± 0.002	1.051 ± 0.003
G2	1.053 ± 0.001	1.047 ± 0.001	1.047 ± 0.010	1.050 ± 0.002
G3	1.053 ± 0.001	1.048 ± 0.001	1.053 ± 0.004	1.050 ± 0.002

Table S4. Arrhenius-model results for potential CH_4 production, sediment–water CH_4 fluxes, and dissolved CH_4 concentrations.

Process	n	Ea (eV)	SE (eV)	95% CI (eV)	R^2	Model p	Increase 10–20 °C
Potential CH_4 production	21	0.81	0.10	0.56–1.03	0.93	<0.001	3.3-fold
Sediment-water CH_4 flux	223	0.94	0.11	0.73–1.16	0.53	<0.001	3.8-fold
Dissolved CH_4	84	1.11	0.07	0.97–1.25	0.80	<0.001	4.9-fold

Note. Models used site-specific intercepts and a common Arrhenius slope. Potential CH_4 production was measured at 3, 10, and 20 °C; sediment-water fluxes and dissolved CH_4 used in situ temperatures.

Table S4a. Combined-model analysis of variance for differences among Arrhenius relationships across processes.

Model term	df	SS	F	p value
Inverse temperature	1	248.90	156.14	3.38×10^{-29}
Process	2	31.585	9.907	6.79×10^{-5}
Site	6	261.14	27.304	5.18×10^{-26}
Inverse temperature × process	2	1.946	0.610	0.544
Process × site	12	54.358	2.842	0.00102
Residual	304	484.59		
Total	327	1187.40		

Table S4b. Pairwise comparisons of Arrhenius relationships among processes with Holm-adjusted p values.

Comparison	Raw p	Holm-corrected p	Significant
Potential CH_4 production vs. sediment-water CH_4 flux	0.697	0.729	No
Sediment-water CH_4 flux vs. dissolved CH_4	0.364	0.729	No
Potential CH_4 production vs. dissolved CH_4	0.0345	0.103	No

Note. The inverse temperature × process interaction was not significant. Holm correction was applied to the three pairwise comparisons.

Table S5. Weighted Deming regression among CH_4-cycling variables and between potential CH_4 production and sediment organic carbon (SOC).

Response vs. predictor	n	Slope	SE	95% CI	R^2g	F	Model p	Slope p	p: slope = 1
Sediment-water flux vs. potential CH_4 production	28	1.136	0.180	0.766–1.506	0.730	70.268	7.29×10^{-9}	1.10×10^{-6}	0.455
Dissolved CH_4 vs. sediment-water flux	28	1.036	0.423	0.167–1.904	0.331	12.868	0.00136	0.0213	0.933
Potential CH_4 production vs. SOC	7	1.194	0.633	−0.432–2.820	0.783	18.090	0.00807	0.118	0.771

Note. Fits accounted for uncertainty in both variables. Model p-values refer to the global generalized-R^2 F-test; slope p-values test the slope against zero, and the final column tests the slope against one.

Table S6a. Welch's ANOVA tests of seasonal differences in dissolved CH_4 and sediment-water CH_4 fluxes.

Response	Grouping	Seasons included	F	df1	df2	p value
Dissolved CH_4	All sites	Summer, autumn, winter	41.552	2	11.828	4.47×10^{-6}
Dissolved CH_4	ULC	Summer, autumn, winter	36.498	2	5.866	4.90×10^{-4}
Dissolved CH_4	LLC	Summer, autumn, winter	80.044	2	3.247	0.00173
Sediment-water CH_4 flux	All sites	Summer, autumn, winter	32.567	2	105.370	9.72×10^{-12}
Sediment-water CH_4 flux	ULC	Summer, autumn, winter	28.080	2	59.797	2.52×10^{-9}
Sediment-water CH_4 flux	LLC	Summer, autumn, winter	11.027	2	45.595	1.24×10^{-4}

Table S6b. Pairwise seasonal comparisons of dissolved CH_4 concentrations and sediment-water CH_4 fluxes with Holm-adjusted p values.

Response	Grouping	Comparison	Difference	t	df	Raw p	Holm p	Significant
Dissolved CH_4	All sites	Summer − autumn	1.5859	4.601	11.036	7.57×10^{-4}	0.00151	Yes
Dissolved CH_4	All sites	Summer − winter	2.7669	9.330	11.972	7.67×10^{-7}	2.30×10^{-6}	Yes
Dissolved CH_4	All sites	Autumn − winter	1.1810	3.367	11.289	0.00607	0.00607	Yes
Dissolved CH_4	ULC	Summer − autumn	1.5193	4.489	5.348	0.00550	0.01099	Yes
Dissolved CH_4	ULC	Summer − winter	2.7351	8.909	5.749	1.41×10^{-4}	4.24×10^{-4}	Yes
Dissolved CH_4	ULC	Autumn − winter	1.2158	3.319	5.866	0.01658	0.01658	Yes
Dissolved CH_4	LLC	Summer − autumn	1.6747	3.336	2.139	0.07231	0.14462	No
Dissolved CH_4	LLC	Summer − winter	2.8092	13.713	2.951	9.13×10^{-4}	0.00274	Yes
Dissolved CH_4	LLC	Autumn − winter	1.1345	2.156	2.540	0.13625	0.14462	No
Sediment–water CH_4 flux	All sites	Summer − autumn	2.0565	5.711	92.435	1.36×10^{-7}	2.71×10^{-7}	Yes
Sediment–water CH_4 flux	All sites	Summer − winter	2.3603	7.286	102.210	6.89×10^{-11}	2.07×10^{-10}	Yes

Response	Grouping	Comparison	Difference	t	df	Raw p	Holm p	Significant
Sediment–water CH_4 flux	All sites	Autumn − winter	0.3038	0.763	106.110	0.44741	0.44741	No
Sediment–water CH_4 flux	ULC	Summer − autumn	2.8563	5.430	53.333	1.41×10^{-6}	2.83×10^{-6}	Yes
Sediment–water CH_4 flux	ULC	Summer − winter	3.0596	6.887	61.303	3.54×10^{-9}	1.06×10^{-8}	Yes
Sediment–water CH_4 flux	ULC	Autumn − winter	0.2034	0.373	56.481	0.71076	0.71076	No
Sediment–water CH_4 flux	LLC	Summer − autumn	1.0336	3.614	45.392	7.53×10^{-4}	0.00151	Yes
Sediment–water CH_4 flux	LLC	Summer − winter	1.4278	4.444	45.393	5.63×10^{-5}	1.69×10^{-4}	Yes
Sediment–water CH_4 flux	LLC	Autumn − winter	0.3942	1.287	43.720	0.20472	0.20472	No

Note. Spring was excluded because ULC and LLC were sampled at different times and temperatures. Differences are expressed in the log-transformed response units used in the Welch analyses.

Table S7. Paired comparison of apparent carbon isotope fractionation factors (α_{app}) between water and sediment.

Comparison	n pairs	Water mean ± SD	Sediment mean ± SD	Paired difference ± SD	95% CI	Test	Statistic	p value
Water vs. sediment αapp	28	1.0568 ± 0.0174	1.0522 ± 0.0077	0.0046 ± 0.0157	−0.0015–0.0107	Paired t-test	t(27) = 1.536	0.136

Note. Paired differences did not deviate significantly from normality (Lilliefors p = 0.448). The Wilcoxon signed-rank sensitivity analysis gave p = 0.127.

Table S7a. Fixed-effects analysis of water-column $\delta^{13}C$- CH_4.

Effect	Sum of squares	df	Mean square	F	p value
Site	249.72	6	41.620	3.613	0.0278
Season	207.55	2	103.77	9.009	0.0041
Error	138.23	12	11.519		

Table S7b. Lake-scale comparisons of water-column $\delta^{13}C$-CH_4 between ULC and LLC within individual seasons.

Season	n ULC	n LLC	Mean ULC (‰)	Mean LLC (‰)	ULC − LLC (‰)	F	df	Raw p	Holm p
Summer	4	3	−51.720	−47.932	−3.787	15.957	1, 5	0.0104	0.0311
Autumn	4	3	−48.938	−39.421	−9.517	10.546	1, 5	0.0228	0.0455
Winter	4	3	−45.577	−38.605	−6.972	9.595	1, 5	0.0269	0.0455

Note. The overall site and season effects were significant, but none of the individual pairwise site comparisons was significant after Tukey-Kramer adjustment. The three seasonal basin contrasts were Holm-corrected.

Table S8a. Fixed-effects analysis of sediment $\delta^{13}C$- CH_4.

Effect	Sum of squares	df	Mean square	F	p value
Site	262.80	6	43.799	17.911	3.59×10^{-10}
Season	54.273	2	27.136	11.097	1.35×10^{-4}
Site × season	303.09	12	25.257	10.329	4.87×10^{-9}
Error	102.71	42	2.445		

Table S8b. One-way ANOVA tests of differences in surface-sediment $\delta^{13}C$- CH_4 among sampling sites within each season.

Season	F	df	p value
Summer	25.638	6, 14	8.70×10^{-7}
Autumn	2.941	6, 14	0.0452
Winter	21.442	6, 14	2.64×10^{-6}

Table S8c. Tukey–Kramer pairwise comparisons of surface-sediment $\delta^{13}C\text{-}CH_4$ among sites within individual seasons.

Season	Site 1	Site 2	Difference (‰)	CI lower	CI upper	Adjusted p
Summer	OBG	SIP	-6.302	-8.925	-3.679	1.6776×10^{-05}
Summer	OBG	MUN	-7.2963	-9.9193	-4.6733	2.9456×10^{-06}
Summer	OBG	LBM	-6.1053	-8.7283	-3.4823	2.4181×10^{-05}
Summer	OBG	G1	-8.2477	-10.871	-5.6247	6.5048×10^{-07}
Summer	OBG	G2	-7.5857	-10.209	-4.9627	1.8332×10^{-06}
Summer	OBG	G3	-5.6317	-8.2547	-3.0087	6.018×10^{-05}
Autumn	SIP	G1	-5.4073	-10.701	-0.11364	0.043868
Winter	OBG	LBM	-10.28	-14.983	-5.5769	4.9304×10^{-05}
Winter	SIP	MUN	-5.3677	-10.071	-0.66453	0.020938
Winter	SIP	LBM	-14.928	-19.631	-10.225	5.7834×10^{-07}
Winter	SIP	G1	-5.0877	-9.7908	-0.38453	0.030283
Winter	SIP	G3	-4.708	-9.4111	-0.0048586	0.049687
Winter	MUN	LBM	-9.5603	-14.263	-4.8572	0.0001097
Winter	LBM	G1	9.8403	5.1372	14.543	8.0054×10^{-05}
Winter	LBM	G2	10.613	5.9099	15.316	3.4432×10^{-05}
Winter	LBM	G3	10.22	5.5169	14.923	5.2638×10^{-05}

Table S8d. Lake-scale comparisons of surface-sediment $\delta^{13}C$-CH_4 between ULC and LLC within individual seasons.

Season	n ULC	n LLC	Mean ULC (‰)	Mean LLC (‰)	ULC − LLC (‰)	F	df	Raw p	Holm p
Summer	4	3	−52.775	−50.546	−2.229	1.155	1, 5	0.3316	0.6631
Autumn	4	3	−54.468	−51.990	−2.478	4.929	1, 5	0.0771	0.2314
Winter	4	3	−53.367	−54.899	1.532	0.171	1, 5	0.6967	0.6967

Note. Only significant Tukey-Kramer site contrasts are shown in Table S8c; all omitted pairwise comparisons had adjusted $p \geq 0.05$. Basin contrasts were Holm-corrected across the three seasons.

Table S9a. Spatial heterogeneity among sampling sites.

Variable	ULC result	Holm-adjusted p	LLC result	Holm-adjusted p
Potential CH_4 production	SIP and MUN > OBG and LBM; SIP = MUN; OBG = LBM	Significant contrasts ≤0.0021; non-significant contrasts ≥0.107	No differences among G1, G2, and G3	1.000
Sediment–water CH_4 flux	SIP and MUN > OBG and LBM; SIP = MUN; OBG = LBM	Significant contrasts $\leq 3.14 \times 10^{-7}$; non-significant contrasts = 1.000	No differences among G1, G2, and G3	≥0.744
Dissolved CH_4	No differences among OBG, SIP, MUN, and LBM	≥0.932	No differences among G1, G2, and G3	1.000

Table S9b. Random-effects comparisons between the Upper Lake Constance (ULC) and Lower Lake Constance (LLC) basins.

Variable	Comparison	p	Interpretation
Potential CH_4 production	ULC vs LLC	0.515	No significant difference
Sediment-water CH_4 flux	ULC vs LLC	0.139	No significant difference
Dissolved CH_4 concentration	ULC vs LLC	0.004	Significantly higher in LLC

Supplementary figures

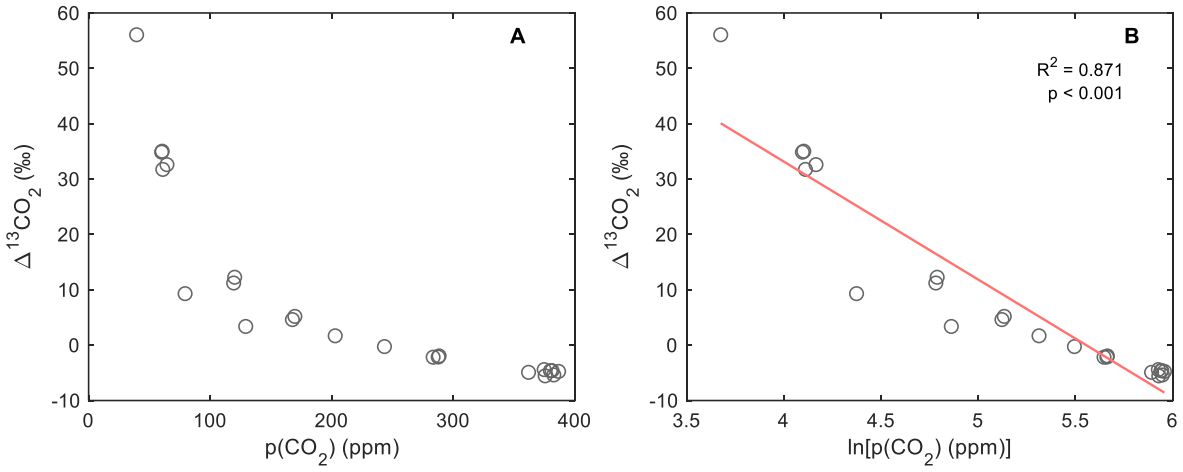

Figure S1. Concentration dependence of cavity ring-down spectroscopy (CRDS) δ^{13}C-CO_2 measurements below 400 ppm CO_2: (a) δ^{13}C-CO_2 versus $p(CO_2)$ and (b) δ^{13}C-CO_2 versus $\ln[p(CO_2)]$. The red line shows the empirical fit $\Delta\ \delta^{13}$C-$CO_2 = -22.191 \times \ln[p(CO_2)] + 124.09$ ($R^2 = 0.873$).

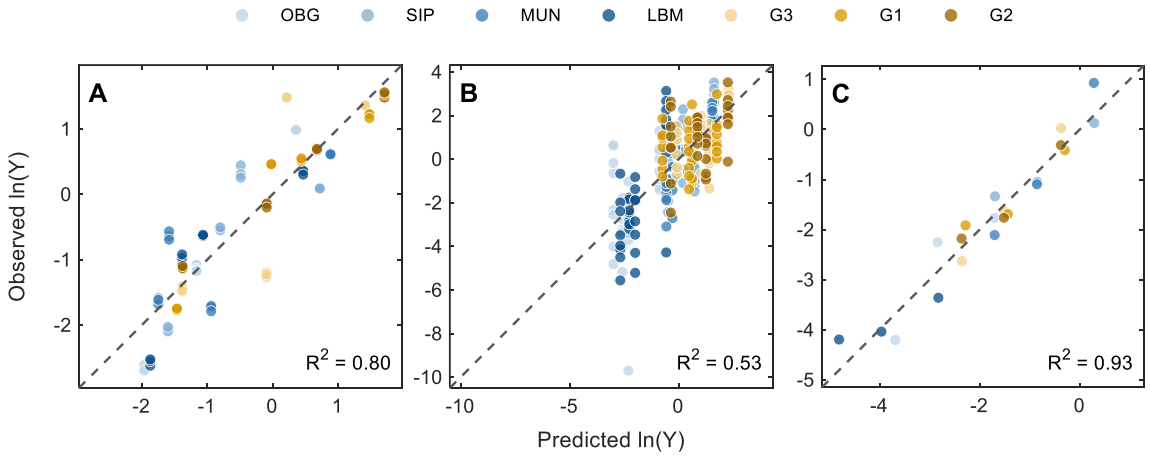

Figure S2. Observed versus predicted values from temperature-response models for (a) dissolved CH_4 concentrations, (b) sediment-water CH_4 fluxes, and (c) potential CH_4 production. Colours identify sampling sites: blue denotes Upper Lake Constance (ULC) and gold denotes Lower Lake Constance (LLC). The dashed line is the 1:1 relationship; R^2 values are shown in each panel.

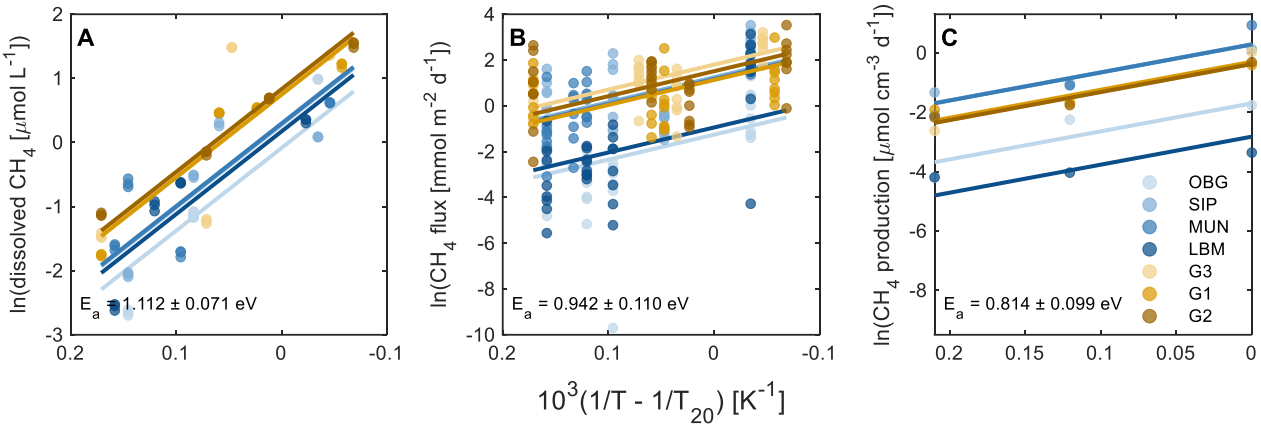

Figure S3. Temperature dependence of CH_4-cycling processes. Linearized Arrhenius plots show the temperature dependence of (a) dissolved CH_4 concentrations, (b) sediment–water CH_4 fluxes, and (c) potential CH_4 production across sites and seasons. A common activation-energy slope was fitted across sites with site-specific intercepts. The x axis is reversed. Estimated activation energies (E_a; mean ± SE) are shown in each panel.

References

Conrad, R., Claus, P., and Casper, P.: Characterization of stable isotope fractionation during methane production in the sediment of a eutrophic lake, Lake Dagow, Germany, Limnol. Oceanogr., 54, 457–471, https://doi.org/10.4319/lo.2009.54.2.0457, 2009.

Uhlig, C. and Loose, B.: Using stable isotopes and gas concentrations for independent constraints on microbial methane oxidation at Arctic Ocean temperatures, Limnol. Oceanogr. Methods, 15, 737–751, https://doi.org/10.1002/lom3.10199, 2017.